Axial Load and Cyclic Lateral Load Tests for Composite Columns with Steel Angles

Hyeon-Jong Hwang[1]; Tae-Sung Eom[2]; Hong-Gun Park, M.ASCE[3]; and Seung-Hwan Lee[4]

Abstract: To enhance the structural capacity and constructability of composite columns, a prefabricated steel-reinforced concrete (PSRC) column was developed. By using the prefabricated steel cage, field rebar work is unnecessary, and the self-erectable steel cage can provide sufficient strength and rigidity to support the construction loads of beams and slabs. In the present study, various steel angle ratios, transverse bar spacings, and prefabrication details were considered for better structural capacity and constructability. To investigate the performance of the proposed method, axial loading tests and cyclic lateral loading tests were performed. In the axial loading test, the structural performance of the PSRC columns was comparable to, or even better than, that of the conventional composite column using the wide flange steel section, when early spalling of the cover concrete was restrained by closely spaced hoops. Under cyclic lateral loading, on the other hand, the PSRC columns were more susceptible to early concrete spalling and steel angle buckling. Thus, when high ductility is required under cyclic lateral loading, the steel angles need to be embedded in the core concrete using thicker cover concrete and hoops. **DOI: 10.1061/(ASCE)ST.1943-541X.0001452.**

Author keywords: Composite column; Compression test; Cyclic test; Seismic test; Steel; Reinforced concrete; Metal and composite structures.

Introduction

In conventional concrete-encased steel (CES) composite columns, a steel section is placed at the center of the cross section [Fig. 1(a)]. Thus, the contribution of the steel section to the overall flexural capacity of the column could be limited. For better efficiency and economy, particularly under biaxial moment, the steel section needs to be placed at the corners, rather than at the center of the cross section (Eom et al. 2014; Hwang et al. 2015; Kim et al. 2008, 2009; Poon 1999; Montuori and Piluso 2009; Campione 2013).

Fig. 1(b) shows an example of such composite columns that was studied by Eom et al. (2014) and Hwang et al. (2015). The prefabricated steel-reinforced concrete (PSRC) column was developed to utilize the advantages of the reinforced concrete column and the steel-concrete composite column: economy and fast construction. In the PSRC column, four steel angles are placed at the corners of the cross section, and transverse bars and plates are used to connect the angles by welding. For convenience in fabrication, the transverse ties can be replaced by continuous hoops [Fig. 1(b); Eom et al. (2013)]. The steel angles resist axial load and flexural moment. The transverse bars and plates provide shear resistance and concrete confinement. To provide a bond between the steel angles and concrete, the transverse reinforcement is welded to the steel angles. Because the steel cage of angles and transverse bars are prefabricated in factories, field rebar work is unnecessary. Further, the self-erectable steel cage can provide sufficient strength and rigidity to support the construction loads of beams and slabs that are superimposed on the column.

Poon (1999), Montuori and Piluso (2009), and Campione (2013) performed compression tests for RC columns strengthened with steel angles (at the four corners of the cross section) and transverse plates (or battens). They used the angles and battens to retrofit existing RC columns. Thus, the angles and battens were exposed without concrete encasement. Poon (1999) performed a concentric compression test. The test result showed that by using the angles and battens, the axial strength and stiffness of the strengthened columns were increased by 20 and 31%, respectively. Montuori and Piluso (2009) performed an eccentric compression test for RC columns strengthened with angles and batten plates. The steel angles and battens confined the core concrete and prevented premature buckling of the longitudinal bars. On the basis of the test results, they proposed a fiber model analysis method for the strengthened RC columns. Campione (2013) studied the buckling of steel angles. The load-carrying capacity and deformation capacity of the strengthened columns increased as the spacing of batten plates decreased.

Kim et al. (2008, 2009) proposed a form-integrated composite column with steel angles and transverse plates, named "yLRC column." In the yLRC column, steel angles were exposed without concrete encasement. As a result, the axial load-carrying capacity was significantly deteriorated by premature buckling of the angles. Eom et al. (2014) performed pure flexural tests for PSRC columns with concrete encasement, to investigate the shear and bond capacities [Fig. 1(b)]. When the specimens were adequately designed for shear and bond, the full flexural capacity was developed after tensile yielding of the steel angles. However, during the post-yield behavior, cover concrete spalling and subsequent bond

[1]Assistant Professor, College of Civil Engineering, Hunan Univ., Yuelu Mountain, Changsha, Hunan 410082, China. E-mail: hwanggun85@naver.com

[2]Assistant Professor, Dept. of Architectural Engineering, Dankook Univ., 152 Jukjeon-ro, Gyeonggi-do 448-701, Korea (corresponding author). E-mail: tseom@dankook.ac.kr

[3]Professor, Dept. of Architecture and Architectural Engineering, Seoul National Univ., 599 Gwanak-ro, Seoul 151-744, Korea. E-mail: parkhg@snu.ac.kr

[4]President, SEN Coretech Inc., 6, Beodeunaru-ro 19 gil, Yeongdeungpo-gu, Seoul 150-040, Korea. E-mail: shlee@senkuzo.com

Note. This manuscript was submitted on November 21, 2014; approved on October 5, 2015; published online on January 5, 2016. Discussion period open until June 5, 2016; separate discussions must be submitted for individual papers. This paper is part of the ***Journal of Structural Engineering***, © ASCE, ISSN 0733-9445.

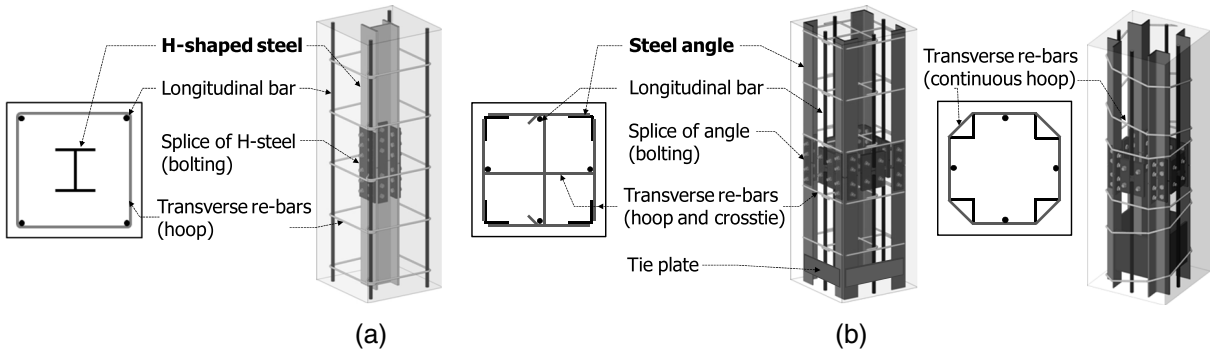

Fig. 1. Concrete-encased composite columns: (a) CES column; (b) PSRC composite column

deterioration occurred between the angles and surrounding concrete.

In the PSRC column and similar columns, the cover concrete can provide local buckling resistance and fire resistance for the steel angles. However, as shown in the previous test results, the load-carrying capacity and deformation capacity of the columns may be limited by early spalling of the cover concrete, particularly when the columns are subjected to repeated cyclic loading or high axial compression force. Further, when transverse bars are welded to steel angles to provide the bond, premature tensile fracture of the weld joint can occur.

In the present study, the axial load and cyclic lateral load behaviors of the PSRC columns were investigated. Two groups of PSRC column specimens were prepared. A pure compression test was performed for the first group to investigate the axial load-carrying capacity and the confinement effects of transverse bars. Then, a cyclic lateral loading test was performed for the second group of specimens with various details of angles and transverse bars, to investigate the seismic performance and post-yield behavior.

Compression Test

Test Specimens

Fig. 2 shows the dimensions and details of a conventional CES column (S1) and five PSRC columns (S2–S6) for compression test. The geometric properties of the specimens are presented in Table 1. The test parameters were the steel ratio (= the ratio of the steel section to the gross area of the column section) and the spacing of transverse bars. The overall height of the specimens was 1,500 mm [Fig. 2(a)]. In order to avoid unexpected concrete failure at the top and bottom bearing plates, the top and bottom concrete of the specimens was confined with steel tube sections B-500 × 500 × 12 (S1–S4) and B-400 × 400 × 12 (S5 and S6).

In the conventional CES specimen S1, the cross section was 500 × 500 mm. A wide flange steel section of H-155 × 150 × 10 × 12 [depth × width × web thickness × flange thickness and cross-sectional area = 4,910 mm^2, Fig. 2(b)] was used at the center of the cross section. Four D19 reinforcing steel bars (diameter = 19.1 mm and cross-sectional area = 287 mm^2 each) were used at the corners of the cross section. For transverse reinforcement, conventional hoops of D10 bars (diameter = 9.53 mm and cross-sectional area = 71 mm^2 each) were used at a vertical spacing of $s = 200$ mm, which satisfied the requirement of AISC 360-10 (AISC 2010): $0.5h_{\min} = 250$ mm.

In PSRC specimen S2, four steel angles of L-90 × 90 × 7 [cross-sectional area = 1,223 mm^2 each, Fig. 2(c)] were used at

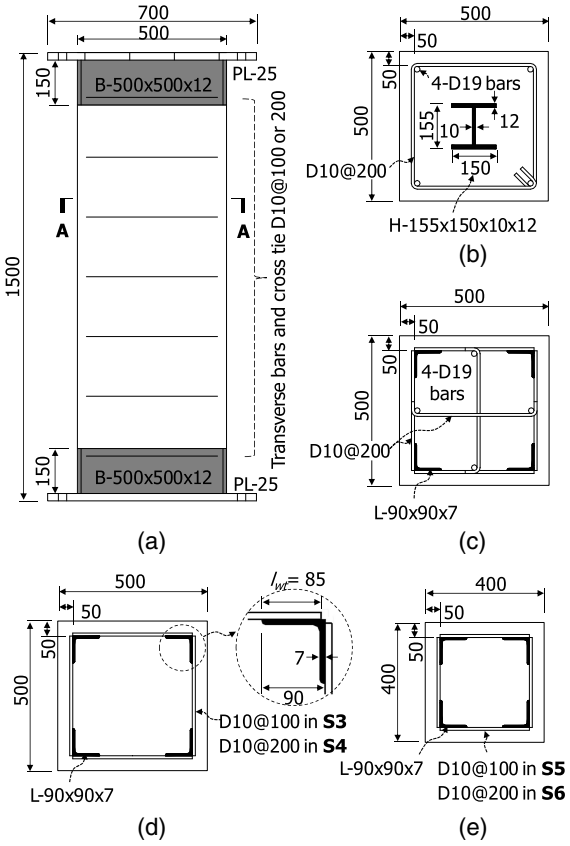

Fig. 2. Dimensions and details of compression test specimens (mm): (a) column configuration; (b) S1 (cross section A-A); (c) S2 (cross section A-A); (d) S3 and S4 (cross section A-A); (e) S5 and S6 (cross section A-A)

the corners of the cross section (500 × 500 mm). The total area of the four angles was equivalent to the area of the H-section used for S1. Four D19 longitudinal bars were placed at the center of the four edges of the cross section. For transverse reinforcement, rectangular hoops were used at a spacing of 200 mm ($s = 200$ mm). Each bar of the hoops (390-mm-long D10 bars) was welded to the surfaces of the angles [weld length $l_w = 85$ mm, Fig. 2(c)]. D10 crossties were also used to laterally support the longitudinal D19 bars.

PSRC specimens S3 and S4 had the same cross section and steel angles (L-90 × 90 × 7) as those of S2 [Fig. 2(d)]. The details of the

Table 1. Specimens for Compression Tests

Specimens	Dimensions (mm)	Steel section [steel ratio (%)]	Longitudinal bars	Hoops (mm)[b]	Crossties (mm)
S1	500 × 500	H-155 × 150 × 10 × 12[a] (2.0)	4-D19	D10 @ 200	—
S2	500 × 500	4 L-90 × 90 × 7 (2.0)	4-D19	D10 @ 200	D10 @ 200
S3	500 × 500	4 L-90 × 90 × 7 (2.0)	N/A	D10 @ 100	—
S4	500 × 500	4 L-90 × 90 × 7 (2.0)	N/A	D10 @ 200	—
S5	400 × 400	4 L-90 × 90 × 7 (3.1)	N/A	D10 @ 100	—
S6	400 × 400	4 L-90 × 90 × 7 (3.1)	N/A	D10 @ 200	—

[a]H-depth × width × web thickness × flange thickness (mm).
[b]Reinforcing steel bars complying with Korean Industrial Standard (diameter = 9.53 mm and cross-sectional area = 71 mm^2 each).

welded rectangular hoops were the same as those of S2. However, in S3 and S4, crossties were not used. The spacings of the hoops were $s = 100$ and 200 mm for S3 and S4, respectively. The hoop spacing of S3 was decreased to 100 mm ($= 0.2h_{min}$) to investigate the effects of the welded rectangular hoops on the axial load behavior of the PSRC column.

Fig. 2(e) shows the cross sections of PSRC specimens S5 and S6. Four angles of L-90 × 90 × 7 were used at the corners of the cross section. As the dimensions of the cross section were decreased to 400 × 400 mm, the steel ratio of S5 and S6 was increased to 3.1%, which was greater than the 2.0% steel ratio of S2 and S3. Each welded rectangular hoop was fabricated with four 290-mm-long D10 bars (weld length $l_w = 85$ mm). The vertical spacing of the hoops were $s = 100$ and 200 mm for S5 and S6, respectively. Crossties were not used.

Materials and Testing Method

To measure the concrete strength, compression tests were performed using concrete cylinders (diameter = 100 mm and height = 200 mm). The concrete strength at the day of column testing was $f'_c = 23.5$ MPa. The yield and tensile strengths of the L-90 × 90 × 7 angles were $F_y = 444$ MPa and $F_u = 689$ MPa, respectively, which were greater than $F_y = 383$ MPa and $F_u = 515$ MPa of H-155 × 150 × 10 × 12, respectively. The yield and tensile strengths were $f_y = 523$ MPa and $f_u = 650$ MPa for D19 bars, respectively, and $f_y = 522$ MPa and $f_u = 654$ MPa for D10 bars, respectively. The reinforcing bars were weldable deformed bars specified in the Korean Building Code (AIK 2009).

Flare-bevel-groove welding (a welding method for connecting a round bar and a flat plate) was used in the connection between the steel angles and transverse bars, following the weld joint details and welding method specified in ANSI/AWS D1.4 (AWS 1998). YFW-C50DR electrodes ($F_{EXX} = 584$ MPa and CVN 86 J at 0°C) were used for the welding. AWS D1.1 (AWS 2010) requires preheating to 60–160°C for the high-strength steel. In the present study, however, preheating was not used.

Fig. 3 shows the test setup for the compression tests of S1–S6. The column specimens were mounted on a pin joint at the base, and axial load was then applied to the top of the column without eccentricity using a 10,000 kN universal testing machine. The effective height of the specimens between the top and bottom pin joints was $H_e = 1{,}820$ mm. Axial shortening of the columns was measured from the LVDTs located at the four corners of the column.

Test Results and Discussion

Fig. 4 shows the axial load-strain (P-ε) relationships of S1–S6. The axial strain ε was calculated by dividing the average shortening measured from the four LVDTs by the net column height [$= 1{,}500 - 2 \times 25$ mm, Fig. 2(a)]. The peak strength P_u, axial strain ε_o at P_u, and ultimate strain ε_u at the failure of the specimen

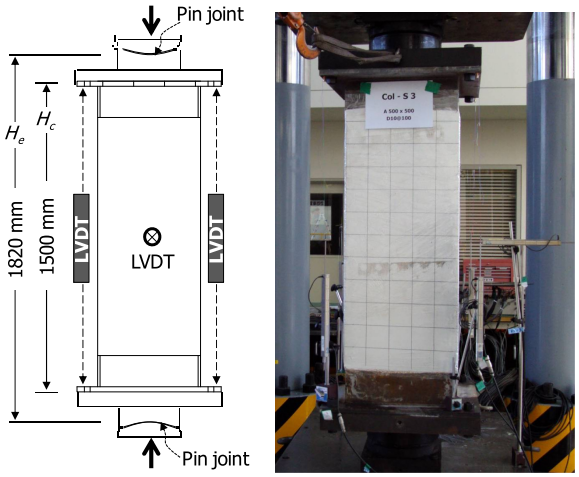

Fig. 3. Setup for compression tests (mm)

are summarized in Table 2. The ultimate strain ε_u was defined as the post-peak strain corresponding to 75% of the peak strength P_u.

The conventional CES specimen S1 showed the peak strength $P_u = 7{,}612$ kN at axial strain $\varepsilon_o = 0.0025$, and ultimately failed at $\varepsilon_u = 0.0041$ [Fig. 4(a)]. After the peak strength, significant strength degradation occurred in the post-peak behavior of S1, due to the relatively large vertical spacing of the hoops.

As shown in Figs. 4(b–f), the axial load behavior of PSRC specimens S2–S6 was similar to that of S1. The peak strengths P_u varied from 5,680 to 8,081 kN depending on the properties of the cross sections. The strains at P_u were slightly increased to $\varepsilon_o = 0.0029$–0.0033, except for S4. The post-peak strength degradation in S2–S6 was not as significant as that of S1. As a result, the ultimate strains at failure were also increased to $\varepsilon_u = 0.0050$–0.0081.

In S2 [Fig. 4(b)], early spalling of the cover concrete occurred at the axial load of 3,000 kN, which decreased the stiffness. However, the peak strength and the ultimate strain were greater than those of the conventional CES column S1, because of the greater yield strength of the steel angles and the lateral confinement provided by the angles. Figs. 4(c and d) show that the peak strength of S3 with closely spaced hoops ($s = 100$ mm) was 14.4% greater than that of S4 with a greater hoop spacing of $s = 200$ mm. A similar result was also seen in the test results of S5 and S6 with different hoop spacings, though the difference in the peak strength was not as significant [Figs. 4(e and f)]. Furthermore, the deformation capacity of S3 and S5 was increased because of the closely spaced hoops.

In this test, local buckling of the steel angles was not observed even at the end of the tests. However, in all specimens, significant

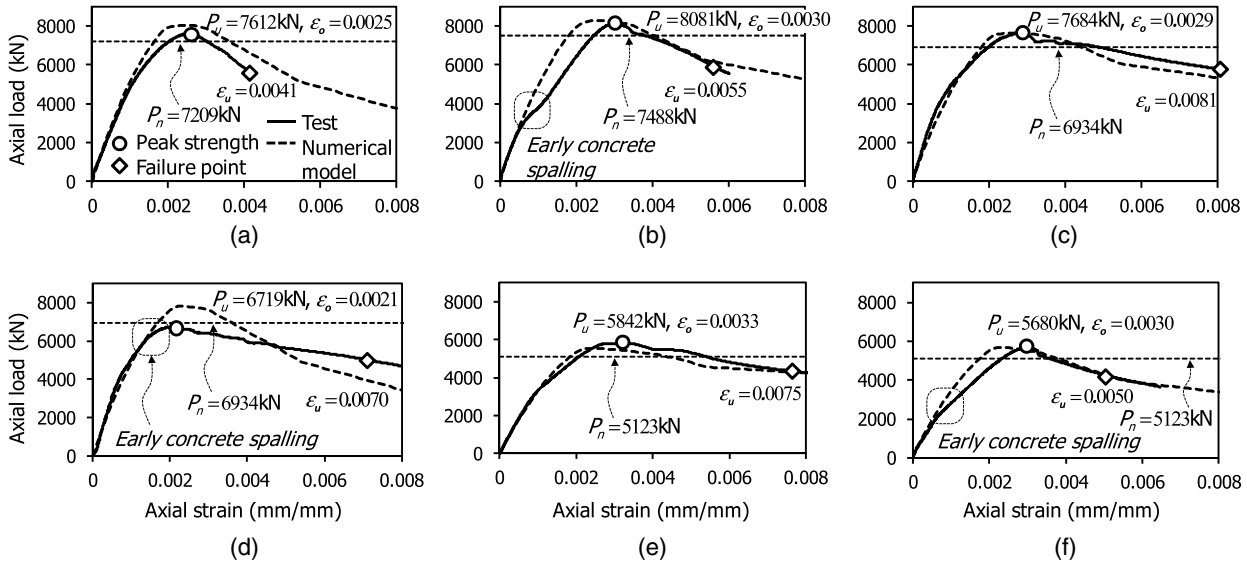

Fig. 4. Axial load-strain relationships of specimens: (a) S1; (b) S2; (c) S3; (d) S4; (e) S5; (f) S6

Table 2. Results of Compression Tests

Specimens	Test results			Predictions Eq. (1)	
	P_u (kN)	ε_o	ε_u	P_n (kN)	P_u/P_n
S1	7,612	0.0025	0.0041	7,209	1.06
S2	8,081	0.0030	0.0055	7,488	1.08
S3	7,684	0.0029	0.0081	6,834	1.12
S4	6,719	0.0021	0.0070	6,934	0.97
S5	5,842	0.0033	0.0075	5,123	1.14
S6	5,680	0.0030	0.0050	5,123	1.11

Note: ε_o = axial strain at the peak strength; ε_u = ultimate strain at failure.

cracking and subsequent concrete spalling occurred after the peak strengths. Particularly, in S2 and S6, concrete spalling occurred early at the level of service loading. Also in S4, the concrete spalling occurred before the peak strength. The early spalling was initiated at the corners of the cross section because of the smooth surface of the angle. This result indicates that hoop bars should be closely spaced, to develop the peak strength by restraining early spalling of the cover concrete. On the basis of the test results, it is recommended that the spacing of hoops be decreased to half of the requirement of conventional CES columns ($s = 0.25h_{\min}$) in order to secure robust axial load behavior of the PSRC columns under high axial load. Alternatively, additional corner ties surrounding the steel angle can be added to prevent the early spalling of cover concrete. Otherwise, the contribution of the cover concrete at the corners to the nominal strength needs to be neglected in the column design.

Axial Load-Carrying Capacity

The nominal compressive strengths P_n of the specimens were evaluated according to AISC 360-10 (AISC 2010), as follows:

$$P_n = P_0 \cdot 0.658^{(P_0/P_e)} \tag{1}$$

in which

$$P_o = 0.85f'_c(A_g - A_s - A_{sr}) + F_yA_s + f_{yr}A_{sr} \tag{2}$$

$$P_e = \pi^2(EI_{\text{eff}})/(KL)^2 \tag{3}$$

$$EI_{\text{eff}} = E_sI_s + 0.5E_sI_{sr} + C_1E_cI_c \tag{4}$$

$$C_1 = 0.1 + 2A_s/(A_c + A_s) \le 0.3 \tag{5}$$

in which P_o = maximum compressive strength of the composite column; P_e = elastic buckling strength of the column; f'_c = concrete strength; F_y and A_s = yield strength and area of the steel section, respectively; f_{yr} and A_{sr} = yield strength and area of the longitudinal bars, respectively; EI_{eff} = effective flexural stiffness of the composite column; KL = effective buckling length; E_s = elastic modulus of steel; E_c = elastic modulus of concrete ($= 4{,}700\sqrt{f'_c}$); I_s, I_{sr}, and I_c = second-order moments of inertia of the steel section, reinforcing bar, and concrete, respectively, with respect to the centroid of the column section; and A_c = concrete area.

Table 2 presents the predicted strengths P_n of the specimens. For the prediction, $H_e = 1{,}820$ mm (Fig. 3) was used for the effective buckling length KL, and the actual material strengths were used. In Table 2, the test peak strengths P_u were 6–14% greater than the predicted strengths P_n, except for S4. In PSRC specimen S4, which had no crossties and a relatively large hoop spacing ($s = 200$ mm), the nominal strength was not fully developed because of early spalling of the concrete.

Nonlinear numerical analysis was performed for the cross section of the test specimens, assuming a perfect bond between the steel and concrete. For the steel sections and reinforcing bars, the stress-strain relationships were idealized as the elastic–perfectly plastic behavior. For the unconfined concrete, a parabolic model proposed by Hognestad (1951) was used. For the confined concrete, a stress-strain relationship proposed by Hoshikuma et al. (1997) was used (Fig. 5)

$$\sigma_{cc}(\varepsilon) = \begin{cases} E_c\varepsilon\left[1 - \frac{1}{n}\left(\frac{\varepsilon}{\varepsilon_{cc}}\right)^{n-1}\right] & \text{for } 0 \le \varepsilon \le \varepsilon_{cc} \\ f'_{cc} - E_{\text{des}}(\varepsilon - \varepsilon_{cc}) & \text{for } \varepsilon_{cc} \le \varepsilon \le \varepsilon_{cu} \end{cases} \tag{6}$$

in which

$$n = \frac{E_c\varepsilon_{cc}}{E_c\varepsilon_{cc} - f'_{cc}} \tag{7}$$

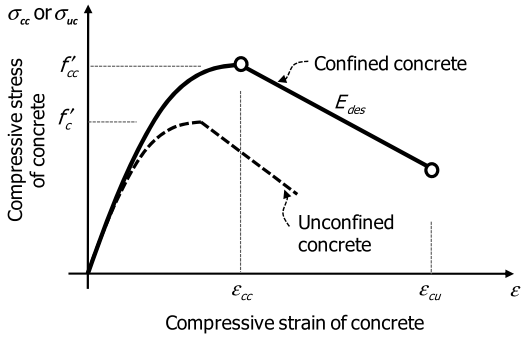

Fig. 5. Stress-strain relationships of confined and unconfined concrete

$$f'_{cc} = f'_c + 0.76\rho_s f_{yh} \tag{8}$$

$$\varepsilon_{cc} = 0.002 + 0.0132\left(\frac{\rho_s f_{yh}}{f'_c}\right) \tag{9}$$

$$\varepsilon_{cu} = \varepsilon_{cc} + \left(\frac{f'_{cc}}{2E_{\text{des}}}\right) \tag{10}$$

$$E_{\text{des}} = 11.2\left(\frac{f'^2_c}{\rho_s f_{yh}}\right) \tag{11}$$

in which ρ_s and f_{yh} = volume ratio and yield strength of the transverse hoop bars, respectively. ρ_s denotes the ratio of the hoop bar volume to the confined concrete volume in a vertical spacing of hoop. For square column sections, ρ_s is the same as the reinforcement ratio of the hoop bars. When $\rho_s = 0$ and $E_{\text{des}} = 0.3E_c$ are used in Eqs. (7)–(11), the stress-strain relationship is equivalent to that of the unconfined concrete.

In Fig. 4, the dashed lines indicate the axial load-displacement relationships obtained from numerical analysis. Generally, the results of numerical analysis correlated well with the test results, from the initial ascending behavior to the post-peak softening behavior. However, in S2 and S6, which suffered early spalling of cover concrete, the test results showed less stiffness than those of the predictions [Figs. 4(b and f)]. In the case of S4, the test peak strength was less than the prediction.

Cyclic Loading Test

The results of the compression test showed that the PSRC columns were vulnerable to premature spalling of cover concrete when hoops were not closely spaced. Thus, under cyclic lateral loading, the PSRC columns were expected to be more susceptible to such damages as the ductility demand increases. Thus, in the cyclic loading test, various details of angles and transverse bars were investigated for better structural capacity.

Test Specimens

Table 3 and Fig. 6 show the details and test parameters of a CES column and three PSRC columns C1–C4 for the cyclic loading test. The cross section and height were 400 × 400 mm and 1,800 mm, respectively. The specimens were subjected to cyclic lateral loading and uniform axial compression. The test parameters were the types of steel sections (i.e., H-section or angle), arrangement of steel angles, types of transverse hoops (i.e., welded rectangular hoop or octagonal continuous hoop), and the use of shear studs between steel sections and concrete.

For the conventional CES specimen C1, a wide flange section of H-150 × 150 × 6 × 9 [cross-sectional area = 3,492 mm^2 and steel ratio = 2.2%, Fig. 6(a)] was used at the center of the cross section, along with four D19 reinforcing bars at the corners. Hoops of D13 bar (diameter = 12.7 mm and cross-sectional area = 127 mm^2) were used for transverse reinforcement. The previous compression test showed the importance of the vertical spacing of the hoops. Thus, for PSRC columns, the vertical spacing of the hoops was decreased to $s = 150$ mm, which was less than the requirement of AISC 360-10 (AISC 2010), $0.5h_{\min}$ (= 200 mm). For comparison, the same spacing ($s = 150$ mm) was used in the CES column. To provide a reliable bond between the steel section and concrete, two ϕ16 shear studs (diameter = 16 mm and cross-sectional area = 201 mm^2) were welded to each flange at a vertical spacing of 200 mm.

For PSRC specimen C2, four steel angles of L-75 × 75 × 6 (cross-sectional area = 873 mm^2 each) were used at the corners of the cross section [Fig. 6(b)]. The total area of the four angles was equivalent to the cross-sectional area of the H-section used in C1. Four D19 longitudinal bars were placed at the center of the edges of the cross section. For transverse reinforcement, tie bars were welded to the steel angles at a spacing of 150 mm. Each of the hoops was fabricated with four 270-mm-long D13 bars [weld length $l_w = 70$ mm, Fig. 2(b)]. The spacing of the hoops ($s = 150$ mm) satisfied the requirement of the bond capacity (between the angles and concrete) that was proposed by Eom et al. (2014). In addition to the hoops, conventional crossties were used.

Figs. 6(c and d) show the details of PSRC specimens, C3 and C4. Four steel angles of L-75 × 75 × 6 were used at the corners of the cross section. However, the angles were rotated 180 degrees so that they were embedded in the core concrete enclosed by the

Table 3. Specimens for Cyclic Lateral Loading Tests

Specimens	Dimensions (mm)	Steel section [steel ratio (%)]	Longitudinal bars	Hoops	Crossties	Tie plates[a]
C1	400 × 400	H-150 × 150 × 6 × 9 (2.2)	4-D19	Conventional hoops D13 @ 150[b]	—	—
C2	400 × 400	4 L-75 × 75 × 6 (2.2)	4-D19	Welded hoops D13 @ 150	D13 @ 150	—
C3	400 × 400	4 L-75 × 75 × 6[c] (2.2)	4-D19	Continuous hoops D13 @ 150	—	8 PL-130 × 250 × 10
C4	400 × 400	4 L-75 × 75 × 6 (2.2)	4-D19	Continuous hoops D13 @ 150	—	8 PL-130 × 250 × 10

[a]At the top and bottom of the column specimens, tie plates were welded transversely to the steel angles.
[b]One-piece rectangular hoops with end seismic hooks were used.
[c]ϕ16 shear studs were welded to each leg of the steel angle at a spacing of 200 mm.

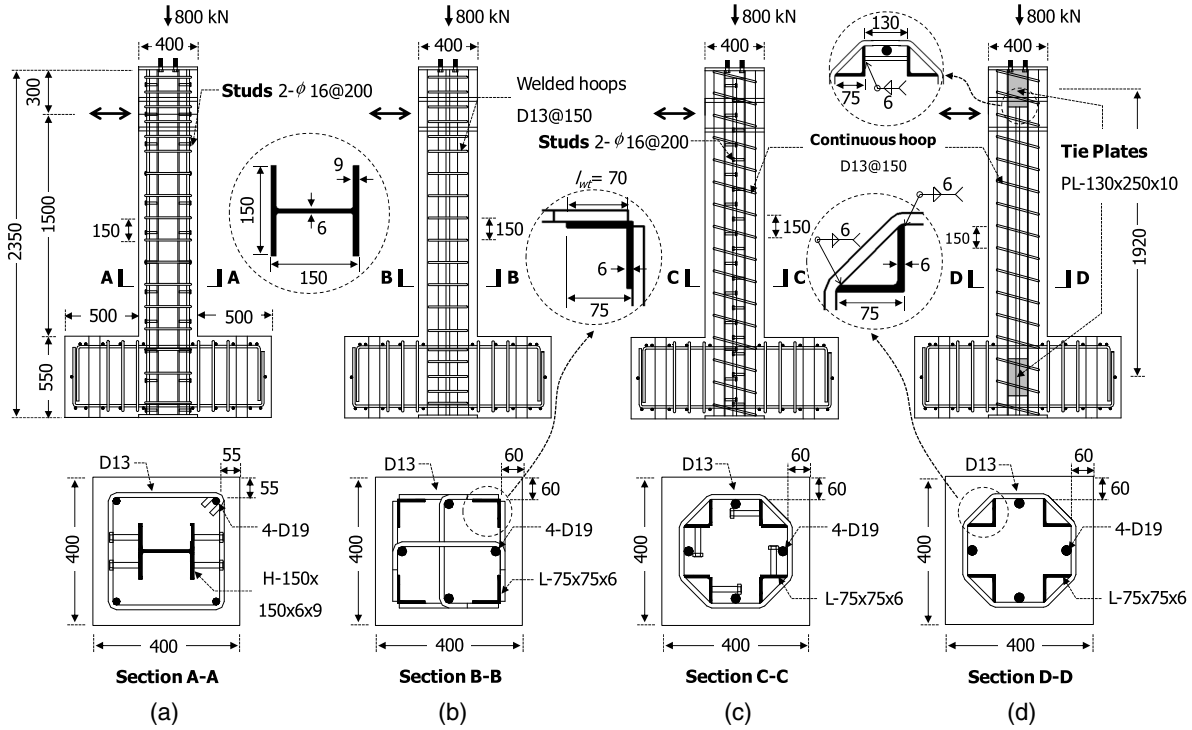

Fig. 6. Dimensions and details of cyclic loading test specimens (mm): (a) C1; (b); C2; (c) C3; (d) C4

hoops. For the hoops, octagonal continuous hoops replaced the welded rectangular hoops. By using the continuous hoops, constructability can be improved [Fig. 6(c)], and lateral confinement for the concrete can be enhanced without anchorage failure of the hoops. Further, by using the thicker cover concrete at the corners of the cross section, spalling of the cover concrete can be restrained.

In C3, for the bond between the angle and concrete, ϕ16 shear studs were welded to each angles at a spacing of 200 mm. In C4, shear studs were not used. Instead, the angles were welded to eight tie plates of PL-130 × 250 × 10 at the top and bottom of the column [fillet weld length = 250 mm each, Fig. 6(d)]. The tie plates were used to provide a bond between the angles and the concrete.

Materials and Testing Method

At the day of the cyclic load test, the concrete strength was $f'_c = 23.3$ MPa. The yield and tensile strengths were $F_y = 402$ MPa and $F_u = 577$ MPa for H-150 × 150 × 6 × 9, $F_y = 477$ MPa and $F_u = 535$ MPa for L-75 × 75 × 6, $F_y = 434$ MPa and $F_u = 544$ MPa for PL-130 × 250 × 10, $f_y = 520$ MPa and $f_u = 629$ MPa for D19 bars, and $f_y = 518$ MPa and $f_u = 646$ MPa for D13 bars, respectively. The tensile strength was $f_u = 440$ MPa for ϕ16 studs. The reinforcing bars used for the tests were weldable deformed bars specified in the Korean Building Code (AIK 2009). In C2, flare-bevel-groove welding was used for the connection between the steel sections and reinforcing bars, following the weld joint details and welding method specified in ANSI/AWS D1.4 (AWS 1998). YFW-C50DR electrodes (F_{EXX} = 584 MPa and CVN 86 J at 0°C) were used for the welding. The same electrode was used for tack welding between the angles and continuous hoops in C3 and C4. Preheating of base metals was not used.

Fig. 7 shows the setup of the cyclic lateral loading test. Two oil jacks were used to apply a uniform axial load of $N = 800$ kN

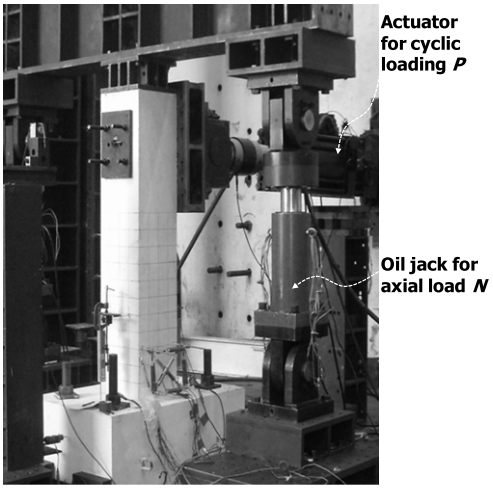

Fig. 7. Test setup of cyclic loading tests

(= $0.224A_g f'_c$, A_g = gross area of column section, f'_c = concrete strength). A cyclic lateral load was applied using an actuator at 1,500 mm from the column bottom. The cyclic loading protocol was planned according to AISC 360-10 (AISC 2010). Deformations were measured at the loading point and the plastic hinge zones. Strain gauges were used to measure the strains of steel angles and transverse hoop bars.

Test Results and Discussions (Load-Displacement Relationship and Damage)

Fig. 8 shows the lateral load–drift ratio (P-δ) relationships of the specimens. The lateral drift ratio was calculated by dividing the net lateral displacement at the loading point by the effective column

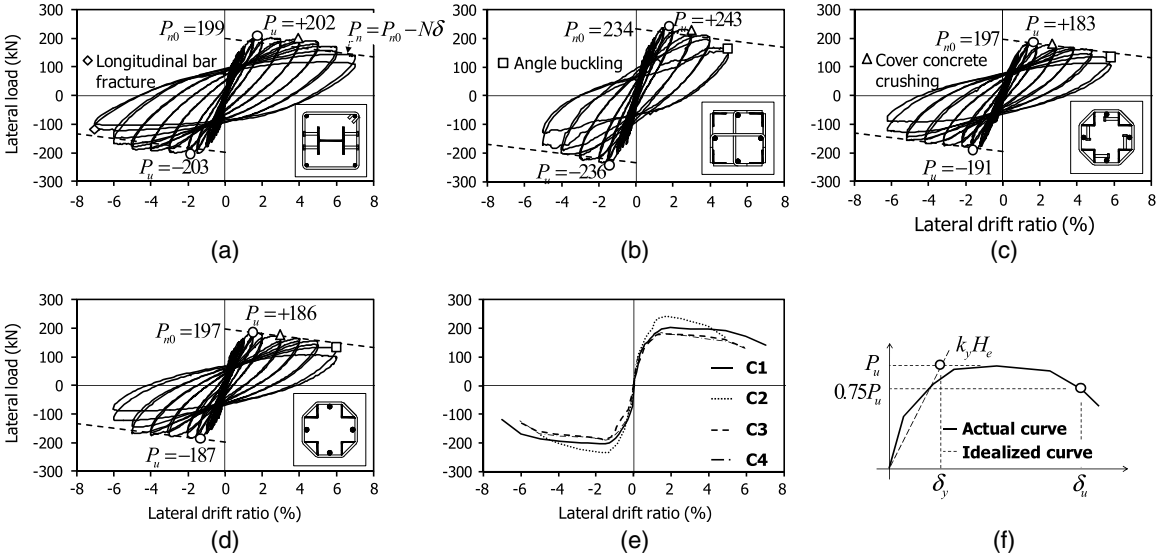

Fig. 8. Lateral load-drift ratio relationships of specimens: (a) C1; (b) C2; (c) C3; (d) C4; (e) envelope curves; (f) definition of yield and maximum drift ratio

height (= 1,500 mm). The peak strength P_u, yield drift ratio δ_y, ultimate drift ratio δ_u, and ductility ratio μ of each specimen are presented in Table 4. As shown in Fig. 8(f), the yield stiffness K_y was defined as the slope corresponding to $0.75P_u$ (Park 1988). The yield drift ratio δ_y was calculated as $\delta_y = P_u/(K_y H_e)$, in which H_e is the shear span length of the specimens (= 1,500 mm). The ultimate drift ratio δ_u was defined as the post-peak drift ratio corresponding to $0.75P_u$. Fig. 9 shows the damage in the plastic hinge regions of the specimens at the end of the tests.

Figs. 8(a) and 9(a) show the test result of the conventional CES specimen, C1. After the peak strength $P_u = +202$ kN at $\delta = 2.0\%$, the load-carrying capacity gradually decreased. Although spalling of the cover concrete occurred at $\delta = 3.0$–4.0% in the plastic hinge region, the load-carrying capacity was not significantly decreased.

Table 4. Summary of Cyclic Loading Test Results

Specimens	Test strength, P_u (kN)		Yield drift ratio, δ_y (%)		Maximum drift ratio, δ_u (%)		Nominal strength, P_{no} (kN)	Yield stiffness, K_y (kN/mm)		Ductility, μ (= δ_u/δ_y)	
	Positive	Negative	Positive	Negative	Positive	Negative		Positive	Negative	Positive	Negative
C1	+202	−203	+0.98	−0.93	+6.01	−6.01	199	13.8 (+)	14.5 (−)	6.13 (+)	6.46 (−)
C2	+243	−236	+1.00	−0.96	+3.98	−4.60	234	16.1 (+)	16.3 (−)	3.98 (+)	4.79 (−)
C3	+183	−191	+0.85	−1.17	+4.81	−5.12	197	14.4 (+)	10.9 (−)	5.66 (+)	4.38 (−)
C4	+186	−187	+0.80	−0.85	+5.00	−5.01	197	15.4 (+)	14.7 (−)	6.25 (+)	5.89 (−)

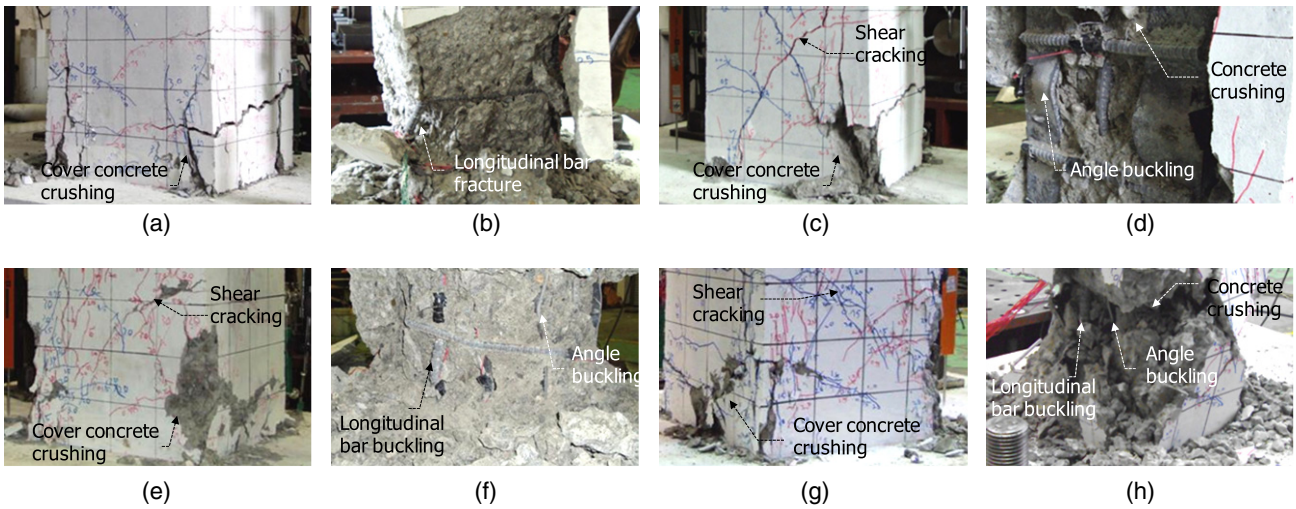

Fig. 9. Damage in plastic hinge regions (cyclic loading tests): (a) C1: 4.0%; (b) C1: 7.0%; (c) C2: 3.0%; (d) C2: 5.0%; (e) C3: 3.0%; (f) C3: 6.0%; (g) C4: 3.0%; (h) C4: 6.0%

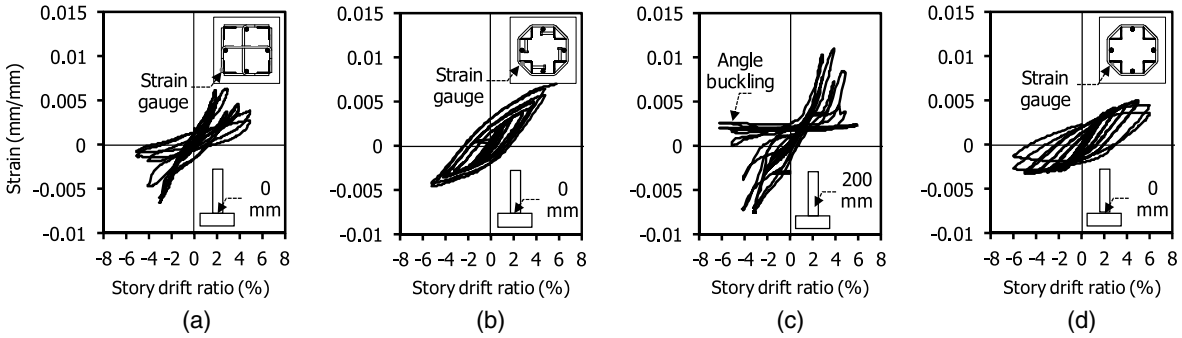

Fig. 10. Strains of steel angles: (a) C2; (b) C3, measured at the base; (c) C3, measured at a height of 200 mm; (d) C4

However, after the spalling of the cover concrete, post-yield buckling occurred in the longitudinal D19 bars. Ultimately, C1 failed at $\delta = 7.0\%$ because of a low cycle fatigue fracture of the longitudinal D19 bars [Fig. 9(b)].

In the PSRC specimen C2, the peak strength was increased to $P_u = +243$ kN at $\delta = 2.0\%$, because of the higher yield strength and the location of the steel angles [Fig. 8(b)]. In Fig. 9(c), at $\delta = 3.0\%$, spalling of the cover concrete occurred, and significant shear cracks occurred in the plastic hinge region because of the increased shear demand. At $\delta = 5.0\%$, the angles and transverse bars were exposed because of the spalling of cover concrete [Fig. 9(d)]. The exposed angles and longitudinal D19 bars were subjected to local buckling during repeated cyclic loading. As a result, the load-carrying capacity of C2 was degraded. However, despite the local buckling of angles and longitudinal bars, tensile fracture did not occur at the weld joint between the angles and transverse bars.

In C3 and C4, where the steel angles were embedded in the core concrete, the peak strengths were significantly decreased to $P_u =$ 183–191 kN because of the reduced moment arm length of the angles compared to that of C2 [Figs. 8(c and d)]. However, in actual columns with large dimensions, the difference in the moment arm length between the C2-type column and C3-type column is not expected to be large. At $\delta = 3.0\%$, spalling of the cover concrete occurred in the plastic hinge region [Figs. 9(e and g)]. However, because of the decreased shear demand (i.e., the decreased peak strength), shear cracking of C3 and C4 was not as significant as that of C2. C3 and C4 exhibited stable cyclic behavior without significant strength and stiffness degradations until large inelastic drift ratios greater than $\delta = 5.0\%$ [Figs. 9(f and h)]. Three possible reasons can explain the enhanced deformation capacity of C3 and C4: (1) the peak strength was less than that of C2; (2) the thickness of the cover concrete was greater and the buckling and bond-slip of the angles were thus more restrained; and (3) the continuous hoops provide better lateral confinement for the concrete (Mander et al. 1988; Hoshikuma et al. 1997). Ultimately, C3 and C4 failed at $\delta =$ 5.0% because of buckling of the angles and longitudinal bars, and subsequent crushing of the confined concrete.

Strains of Steel Angles and Transverse Hoops

Fig. 10 shows the longitudinal strains of the steel angles in C2–C4. The strains were measured from strain gauges located at the heights of 0 and 200 mm from the column base. In Fig. 10(a), the strain of C2 measured at the column base increased in proportion to the drift ratios until $\delta = 3.0\%$. However, the strain began to decrease as the buckling of angles occurred. Figs. 10(b and c) show the angle strains of C3 measured at the column base and a height of 200 mm, respectively. Fig. 10(b) shows that the strain at the column base increased proportionally to the lateral drift ratios, showing relatively large energy dissipation. On the other hand, in Fig. 10(c), the strain measured at 200 mm from the column base significantly decreased at $\delta = 5.0\%$ because of buckling of the angles, showing a small residual strength during the subsequent load cycles. Due to the buckling of the angles, the strain at the column base also showed a small value. Fig. 10(d) shows that the strain of the angle in C4 at the column base was very close to that of C3 shown in Fig. 10(b). However, the maximum and minimum values of the angle strain in C4 were slightly less than those of C3. The reduced angle strain of C4 is attributed to the bond-slip of the angles embedded in concrete: In C4, shear studs were not used for the angles; thus, the bond-slip at the interface between the angles and concrete was unavoidable, although the effect of the bond-slip on the overall cyclic behavior was not significant [Fig. 8(d)].

Fig. 11 shows the strains of the transverse bars measured at 50 mm from the column base. The bar strain of the conventional CES specimen C1 was the smallest. This is because the shear force applied to the steel section was resisted by the web of the steel section, rather than by the transverse bars. In contrast, the bar strain of the PSRC specimen C2 was the greatest, and larger than the yield strain [Fig. 11(b)]. In the PSRC columns, transverse hoops should provide shear resistance as well as concrete confinement. Further, the shear demand of C2 was 20% greater than that of C1. Therefore, the bar strain of C2 was significantly increased. As shown in Figs. 11(c and d), the bar strains of C3 and C4 were less than that of C2 and the yield strain. This is because the shear demands were 25% less than that of C2. This test result indicates that in PSRC columns, the hoops should be sufficiently closely spaced to provide shear resistance and lateral confinement.

Yield Stiffness

Table 4 presents the yield stiffness K_y of the specimens. As shown in Fig. 8(f), the yield stiffness K_y was defined by dividing the peak strength P_u by the yield displacement Δ_y $(= \delta_y H_e)$. The yield stiffness of the PSRC specimen C2 ($K_y = 16.1$ and 16.3 kN/mm) was on average 14.6% greater than that of the CES specimen C1 ($K_y = 13.8$ and 14.5 kN/mm). This is because the angles placed at the corners of the cross section increased the flexural stiffness of C2. However, in C3 and C4, where the angle sections were rotated 180 degrees, the yield stiffness was equivalent to that of C1. The yield stiffness of C4 without shear studs was comparable to that of C3 with shear studs.

Deformation Capacity

Table 4 presents the maximum drift ratios δ_u and ductility ratios μ $(= \delta_u/\delta_y)$ of C1–C4. The maximum drift ratios δ_u and ductility

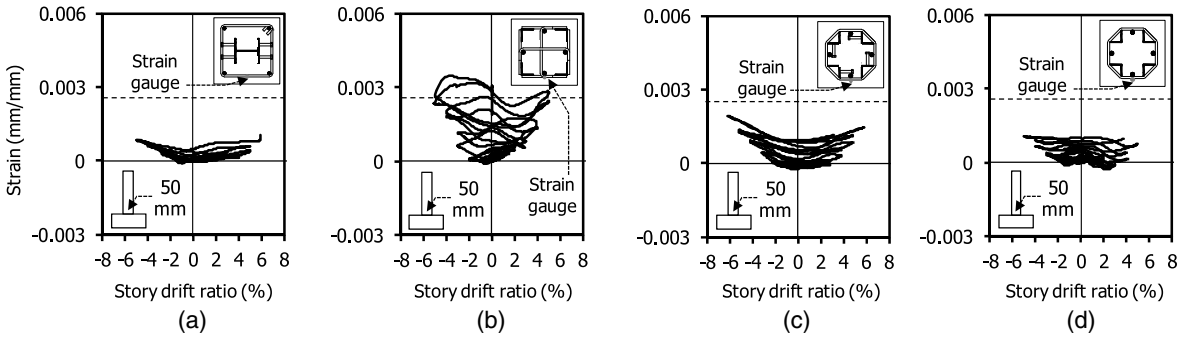

Fig. 11. Strains of transverse bars: (a) C1; (b) C2; (c) C3; (d) C4

ratios μ ($= \delta_u/\delta_y$) of the specimens exceeded 3.98% and 3.98, respectively, which indicates that despite the compression force $N = 800$ kN ($= 0.224A_g f'_c$), the specimens exhibited relatively high deformation capacities. However, the deformation capacity of each specimen was significantly affected by the type and arrangement of steel sections, as follows.

C1 with H-section exhibited the greatest deformation capacity, $\delta_u = 6.01\%$. On the other hand, PSRC specimen C2 with welded transverse hoops exhibited the least deformation capacity ($\delta_u = 3.98\%$). The lower deformation capacity of C2 is attributed to the following: (1) the high peak strength increased the demand forces for the bond and shear, increasing the diagonal cracks and concrete damages in the plastic hinge region [Fig. 11(b)]; (2) after spalling of the cover concrete, the bond strength between the angles and concrete significantly decreased as the bearing capacity of the cover concrete decreased (Eom et al. 2014); and (3) after the spalling of cover concrete, the steel angles were susceptible to buckling under repeated cyclic loading.

On the other hand, in PSRC specimens C3 and C4, the angles were embedded in the concrete confined with the continuous hoops. Thus, even after the spalling of cover concrete, the bond deterioration and local buckling of the angles were restrained. As a result, the deformation capacities of C3 and C4 ($\delta_u = 4.81$ and 5.00%) were greater than that of C2.

Energy Dissipation Capacity

Fig. 12 shows the variation of energy dissipation capacity according to the lateral drift ratio. In Fig. 12(a), the energy dissipation per load cycle, E_D, was defined as the area enclosed by a full cyclic curve of the second load cycle. C2 exhibited the greatest E_D values until $\delta = 4.0\%$ because of the greater load-carrying capacity. After $\delta = 4.0\%$, however, the increase rate of E_D significantly decreased. On the other hand, in C1, C3, and C4 with the greater deformation capacities, E_D values increased proportionally to the lateral drift ratio until $\delta = 5.0\%$. C1 shows the greatest E_D value. Fig. 12(b) shows the energy dissipation ratios κ at each drift level. κ was defined as the ratio of the actual energy dissipation E_D per load cycle [i.e., E_D values in Fig. 12(a)] to the idealized elastic–perfectly plastic energy dissipation E_{ep}:$\kappa = E_D/E_{ep}$. As shown in Fig. 12(b), the κ values ranged from 0.12 to 0.6 and increased in proportion to the lateral drift ratios.

Verification of Structural Capacity of PSRC Columns

Load-Carrying Capacity

The lateral load-carrying capacities of C1–C4 were evaluated according to AISC 360-10 (AISC 2010). First, the nominal flexural strength M_n was calculated from section analysis considering the effect of compression force $N = 800$ kN ($= 0.224A_g f'_c$). The plastic stress distribution method specified in AISC 360-10 was used for the section analysis. The lateral load-carrying capacity was then calculated as $P_{no} = M_n/H_e$ ($H_e = 1{,}500$ mm). Because the column specimens were subjected to compression force $N = 800$ kN, the actual lateral load-carrying capacity was decreased by the second-order effect. Therefore, the nominal strength P_n was calculated as follows:

$$P_n = P_{no} - N\delta \tag{12}$$

in which δ = lateral drift ratio of the specimens.

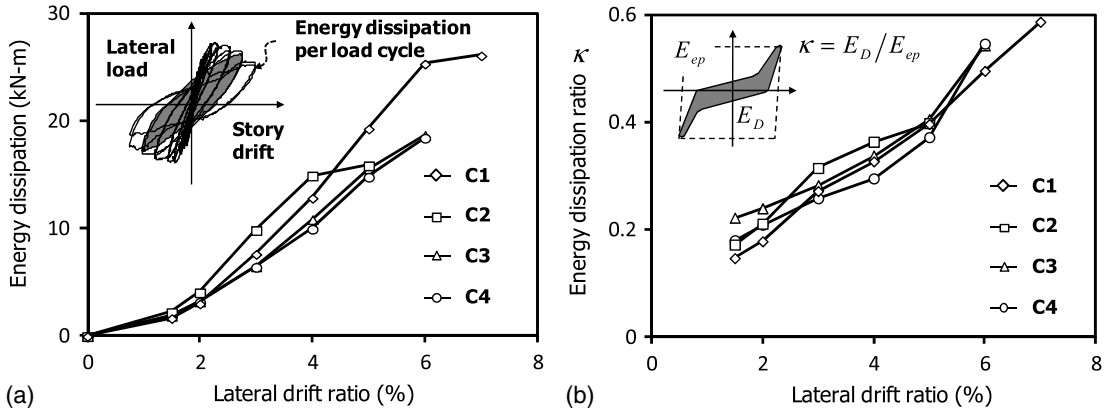

Fig. 12. Energy dissipation per load cycle

The lateral load-carrying capacities, P_{no} and P_n, of the specimens are presented as the dotted lines in Figs. 8(a–d). The predicted strengths, P_n, decreased as the lateral drift ratio increased because of the second-order effect. The predictions correlated well with the test results. This result indicates that the flexure-compression strength of the PSRC columns can be successfully predicted according to AISC 360-10 (AISC 2010).

Although the same steel ratio (= 2.2%) was used for C1–C4, the load-carrying capacity was significantly affected by the type and arrangement of the steel sections. The PSRC specimen C2, which had four angles at the corners of the cross section, showed the greatest strengths. In C3 and C4, the test strengths and predicted strengths were about 20% less than that of C2 because the centroid of the steel angles was positioned closer to the center of the cross section. The load-carrying capacity of the CES specimen C1 was about 16% less than that of C2. The lower strength of C1 is attributed to the location and lower yield strength of the H-section. The yield strength ($F_y = 402$ MPa) of the H-section in C1 was less than that of the angles (477 MPa) in C2, which accounted for a 7.4% decrease in the strength. By placing the H-section at the center of the cross section, the strength was again decreased by 8.6%. If a flexural moment is applied to the weak axis, the load-carrying capacity of C1 is further decreased, which is about 25% less than that of C2.

Shear Strength

The shear resistance of PSRC columns is provided by concrete, transverse bars, and steel angles. Because the dimensions of the angle cross section are significantly less than those of the entire cross section, the contribution of the angles can be neglected (Eom et al. 2014). Therefore, according to ACI 318-11 (ACI 2011), the nominal shear strength V_n of the PSRC columns is calculated, considering the contributions of concrete and transverse bars

$$V_n = \frac{1}{6}\sqrt{f'_c}bd + A_{sh}f_{yh}\frac{d}{s} \le \frac{5}{6}\sqrt{f'_c}bd \tag{13}$$

in which b = width of the cross section; d = effective depth of the cross section (i.e., distance from the end of the concrete compression zone to the geometric center of the tension angles); and A_{sh}, f_{yh}, and s = area, yield stress, and spacing of the transverse bars, respectively.

In all specimens, the nominal shear strengths predicted using Eq. (13) were greater than the shear demand ($V_n/V_u = 2.02$ for C1, 2.25 for C2, 2.13 for C3, and 2.18 for C4). For this reason, shear failure did not occur in the test specimens.

Bond Resistance

Eom et al. (2014) investigated the bond resistance T_{bn1} between steel angle and concrete, which is provided by the bearing action of the transverse bars welded to the angle. In the present study, in addition to the bearing strength T_{bn1}, the friction bond strength T_{bn2} (CEB-FIP 1993) and shear stud strength T_{bn3} [Specimen C3, AIK 2009; AISC 360-10 (AISC 2010)] were considered

$$T_{bn1} = 2\left[0.85f'_c(2d_{bh}l_{wh})\left(\frac{l_s}{s}\right)\right] \tag{14}$$

$$T_{bn2} = 0.05\sqrt{f'_c}D_A l_s \tag{15}$$

$$T_{bn3} = 0.5A_{sc}\sqrt{f'_c E_c}n_s \tag{16}$$

Table 5. Evaluation of Bond Strength

Specimens	Bond capacity				
	T_{bn1} (kN)	T_{bn2} (kN)	T_{bn3} (kN)	T_{bn}	T_{bn}/T_{bu}
C2	721	26	—	721	1.35
C3	62	26	579	579	1.08
C4	62	26	—	62	0.12

Note: $d_{bh} = 13$ mm; $l_s = 1{,}500$ mm; and $l_{wh} = 70$ mm (C2) and 6 mm (C3 and C4).

in which d_{bh} = diameter of a transverse bar; l_{wh} = weld length of a transverse bar; l_s = shear span of the PSRC column (i.e., distance between the critical section and the zero-moment location); D_A = circumference of an angle; A_{sc} = section area of a stud; and n_s = the number of studs in length l_s. In Eq. (15), the friction bond stress between the angle and concrete was defined as $0.05\sqrt{f'_c}$, considering the smooth surfaces of the angle (CEB-FIP 1993). To restrain the bond-slip of the angle, the nominal bond strength T_{bn} should be greater than the bond demand $T_{bu} = 536$ kN, which was defined as 1.3 times the yield strength of the angle, addressing the cyclic strain hardening (= $1.3A_{sa}F_y$; A_{sa} = area of the angle section; Eom et al. 2014). The nominal bond strength T_{bn} was defined as the maximum between T_{bn1}, T_{bn2}, and T_{bn3} [AIK 2009; AISC 360 (AISC 2010)].

For C2, C3, and C4, T_{bn1} was calculated as 721 kN, 62 kN, and 62 kN, respectively. $T_{bn2} = 26$ kN for C2, C3, and C4. $T_{bn3} = 579$ kN for C3 (Table 5). Thus, the bond strengths T_{bn} were estimated as 721, 579, and 62 kN for C2, C3, and C4, respectively. In C2 and C3 with the sufficient strengths ($T_{bn}/T_{bu} = 1.35$ for C2, and 1.08 for C3), the bond-slip of the angle was restrained. In C4 with the insufficient bond strength of $T_{bn}/T_{bu} = 0.12$, local bond slip of the angles was unavoidable. Nevertheless, the lateral load-drift relationship was equivalent to that of C3 with sufficient bond strength. This is because the tie plates at the top and bottom of the column were able to transfer the horizontal shear that was required to develop the tension and compression forces of the steel angles. For the shear transfer, tie plates should be provided at the locations of the maximum and minimum forces of the steel angles.

Summary and Conclusions

In the present study, to investigate the structural capacities of PSRC columns with various details, compression tests and cyclic lateral loading tests were performed. From the test results, the load-carrying capacity, deformation capacity, failure mode, and energy dissipation capacity of the specimens were investigated. The results of the compression test are summarized as follows:

1. In the PSRC specimens (S2–S6) with welded rectangular hoops, the axial load-carrying capacity and deformation capacity were comparable to, or even better than, those of the conventional CES specimen (S1). The axial load-carrying capacities predicted by AISC 360-10 correlated well with the test results. This result indicates that under pure axial loading, the corner angles and the welded hoops provided adequate lateral confinement to the concrete.
2. However, to prevent early spalling of cover concrete at the corners of the cross-section, closely spaced hoops should be provided. It is recommended that under high axial compression, the vertical spacing of hoops is decreased to $s = 0.25h_{\min}$, which is less than the requirement of AISC, $0.5h_{\min}$. Otherwise, additional corner ties surrounding the angle may be required, to restrain early spalling of the cover concrete.

The results of the cyclic loading tests are summarized as follows:

1. Under cyclic lateral loading (uniform compression of $0.22f'_cA_g$), the PSRC specimens (C2–C4) showed deformation capacities of $\delta_u = 4$–5%, which were less than $\delta_u = 6\%$ of the conventional CES specimen (C1).
2. The lower deformation capacity of the PSRC columns is attributed to the following reasons: (1) relatively large plastic strains occur in the corner steel angles; (2) after spalling of the cover concrete, the exposed steel angles are susceptible to local buckling; and (3) the shear demand of the transverse reinforcement increases.
3. The PSRC column C2, which had hoops welded to the corner angles without shear connectors, showed the lowest ductility. On the other hand, the PSRC columns C3 and C4, which had thicker cover concrete at the corners of the cross-sections, shear connectors (or tie plates), and continuous hoops, showed better deformation capacities. This result indicates that when high ductility is required, the steel angles need to be embedded in the core concrete using thicker cover concrete and hoops.
4. The lateral load-carrying capacity of the PSRC columns predicted by AISC 360-10 correlated well with the test strengths.
5. The hoop spacing is recommended to be at least $s = 0.375h_{\min}$, which is less than the minimum requirement for conventional CES columns ($= 0.5h_{\min}$). For more reliable performance, the hoop spacing may be decreased to $s = 0.25h_{\min}$, which is the recommendation resulting from the pure compression test.

Acknowledgments

This research was financially supported by grants from the R&D Policy Infra Program (Code 11-Technology Standardization-09-01) funded by the Ministry of Land, Transportation, and Maritime Affairs of Korea; the Small and Medium Business Administration in Korea (No. 00045821); and the Basic Science Research Program through the National Research Foundation of Korea (NRF) funded by the Ministry of Education, Science, and Technology (2012R1A1A1003282). The authors are grateful to the authorities for their support.

References

ACI (American Concrete Institute). (2011). "Building code requirements for structural concrete and commentary." *ACI 318-11*, Farmington Hills, MI.

AIK (Architectural Institute of Korea). (2009). "Korean building code." Seoul.

AISC. (2010). "Specification for structural steel building." *ANSI/AISC 360-10*, Chicago.

AWS (American Welding Society). (1998). "Structural welding code-reinforcing steel." *AWS D1.4*, Miami.

AWS (American Welding Society). (2010). "Structural welding code-steel." *AWS D1.1*, Miami.

Campione, G. (2013). "R/C columns strengthened with steel angles and battens: Experimental results and design procedure." *Pract. Period. Struct. Des. Constr.*, 10.1061/(ASCE)SC.1943-5576.0000125, 1–11.

CEB-FIP (Comité Euro-International-Fédération International de la Précontrainte). (1993). "CEB-FIP model code 1990: Design code." Thomas Telford, London, 437.

Eom, T. S., Hwang, H. J., Park, H. G., Lee, C. N., and Kim, H. S. (2014). "Flexural test for steel-concrete composite members using prefabricated steel angles." *J. Struct. Eng.*, 10.1061/(ASCE)ST.1943-541X.0000898, 04013094.

Eom, T. S., Kang, S. M., Park, H. G., Choi, T. W., and Jin, J. M. (2013). "Cyclic loading test for reinforced concrete columns with continuous rectangular and polygonal hoops." *Eng. Struct.*, 67(5), 39–49.

Hognestad, E. (1951). *Study of combined bending and axial load in reinforced concrete members*, Univ. of Illinois Engineering Experimental Station, 128.

Hoshikuma, J., Kawashima, K., Nagaya, K., and Taylor, A. W. (1997). "Stress-strain model for confined reinforced concrete in bridge piers." *J. Struct. Eng.*, 10.1061/(ASCE)0733-9445(1997)123:5(624), 624–633.

Hwang, H. J., Eom, T. S., Park, H. G., Lee, S. H., and Kim, H. S. (2015). "Cyclic loading tests for beam-column connections of concrete filled u-shaped steel beams and concrete-encased steel angle columns." *J. Struct. Eng.*, 10.1061/(ASCE)ST.1943-541X.0001242, 04015020.

Kim, B. R., Kang, S. D., Kim, H. G., Kim, M. H., and Kim, S. D. (2008). "A study on the fire resistance of yLRC composite columns with steel sheet forms and angles (in Korean)." *J. Korean Soc. Steel Constr.*, 20(3), 365–375.

Kim, H. G., Kim, M. H., Cho, N. G., Kim, S. S., and Kim, S. D. (2009). "Experimental study on the compressive strength of yLRC composite columns (in Korean)." *J. Korean Soc. Steel Constr.*, 21(5), 545–552.

Mander, J. B., Priestley, M. J. N., and Park, R. (1988). "Theoretical stress-strain model for confined concrete." *J. Struct. Eng.*, 10.1061/(ASCE)0733-9445(1988)114:8(1804), 1804–1826.

Montuori, R., and Piluso, V. (2009). "Reinforced concrete columns strengthened with angles and battens subjected to ecconcentric load." *Eng. Struct.*, 31(2), 539–550.

Park, R. (1988). "State-of-the-art report on ductility evaluation from laboratory and analytical testing." *Proc., 9th World Conf. on Earthquake Engineering*, Vol. 8, International Association for Earthquake Engineering, Tokyo, 605–616.

Poon, E. D. (1999). *Effect of column retrofitting on the seismic response of concrete frames*, Dept. of Civil Engineering and Applied Mechanics, McGill Univ., Montreal, 162.